Computational and Structural Biotechnology Journal 21 (2023) 3466–3477

Contents lists available at ScienceDirect

Computational and Structural Biotechnology Journal

journal homepage: www.elsevier.com/locate/csbj

Single-cell and spatiotemporal transcriptomic analyses reveal the effects of microorganisms on immunity and metabolism in the mouse liver

Ruizhen Zhao [a,b], Wei Cheng [c], Juan Shen [b], Weiming Liang [b], Zhao Zhang [a,b], Yifei Sheng [a,b], Tailiang Chai [a,b], Xueting Chen [a,b], Yin Zhang [a,b], Xiang Huang [a], Huanjie Yang [b], Chunqing Song [d], Li Pang [e], Cuoji Nan [b], Yangrui Zhang [f], Rouxi Chen [f], Junpu Mei [b,f], Hong Wei [g,*], Xiaodong Fang [b,f,**]

[a] College of Life Sciences, University of Chinese Academy of Sciences, Beijing 100049, China
[b] BGI-Shenzhen, Shenzhen 518083, China
[c] College of Animal Sciences and Technology, Huazhong Agricultural University, Wuhan 430070, China
[d] Key Laboratory of Growth Regulation and Translational Research of Zhejiang Province, School of Life Sciences, Westlake University, Hangzhou, Zhejiang 310024, China
[e] BGI-Qingdao, BGI-Shenzhen, Qingdao 266555, China
[f] BGI-Sanya, BGI-Shenzhen, Sanya 572025, China
[g] Precision Medicine Institute, The First Affiliated Hospital, Sun Yat-sen University, Guangzhou, Guangdong 510080, China

ARTICLE INFO

Article history:
Received 17 March 2023
Received in revised form 28 June 2023
Accepted 28 June 2023
Available online 30 June 2023

Keywords:
Gut-liver axis
Germ-free mice
Microbiota
Stereo-seq & sc/snRNA-seq
Immune cell
Metabolism
Liver zonation

ABSTRACT

The gut-liver axis is a complex bidirectional communication pathway between the intestine and the liver in which microorganisms and their metabolites flow from the intestine through the portal vein to the liver and influence liver function. In a sterile environment, the phenotype or function of the liver is altered, but few studies have investigated the specific cellular and molecular effects of microorganisms on the liver. To this end, we constructed single-cell and spatial transcriptomic (ST) profiles of germ-free (GF) and specific-pathogen-free (SPF) mouse livers. Single-cell RNA sequencing (scRNA-seq) and single-nucleus RNA sequencing (snRNA-seq) revealed that the ratio of most immune cells was altered in the liver of GF mice; in particular, natural killer T (NKT) cells, IgA plasma cells (IgAs) and Kupffer cells (KCs) were significantly reduced in GF mice. Spatial enhanced resolution omics sequencing (Stereo-seq) confirmed that microorganisms mediated the accumulation of Kupffer cells in the periportal zone. Unexpectedly, IgA plasma cells were more numerous and concentrated in the periportal vein in liver sections from SPF mice but less numerous and scattered in GF mice. ST technology also enables the precise zonation of liver lobules into eight layers and three patterns based on the gene expression level in each layer, allowing us to further investigate the effects of microbes on gene zonation patterns and functions. Furthermore, untargeted metabolism experiments of the liver revealed that the propionic acid levels were significantly lower in GF mice, and this reduction may be related to the control of genes involved in bile acid and fatty acid metabolism. In conclusion, the combination of sc/snRNA-seq, Stereo-seq, and untargeted metabolomics revealed immune system defects as well as altered bile acid and lipid metabolic processes at the single-cell and spatial levels in the livers of GF mice. This study will be of great value for understanding host-microbiota interactions.

1. Introduction

Metabolism and detoxification act as the primary function of the mammalian liver, whereas the intestine's primary function is digestion and absorption. As research continues, the interrelationship between these two organs is gradually being uncovered. First, these organs share a common embryological origin, and previous studies have revealed

* Corresponding author.
** Corresponding author at: BGI-Shenzhen, Shenzhen 518083, China.
E-mail addresses: weihong63528@163.com (H. Wei), fangxd@genomics.cn (X. Fang).

https://doi.org/10.1016/j.csbj.2023.06.020

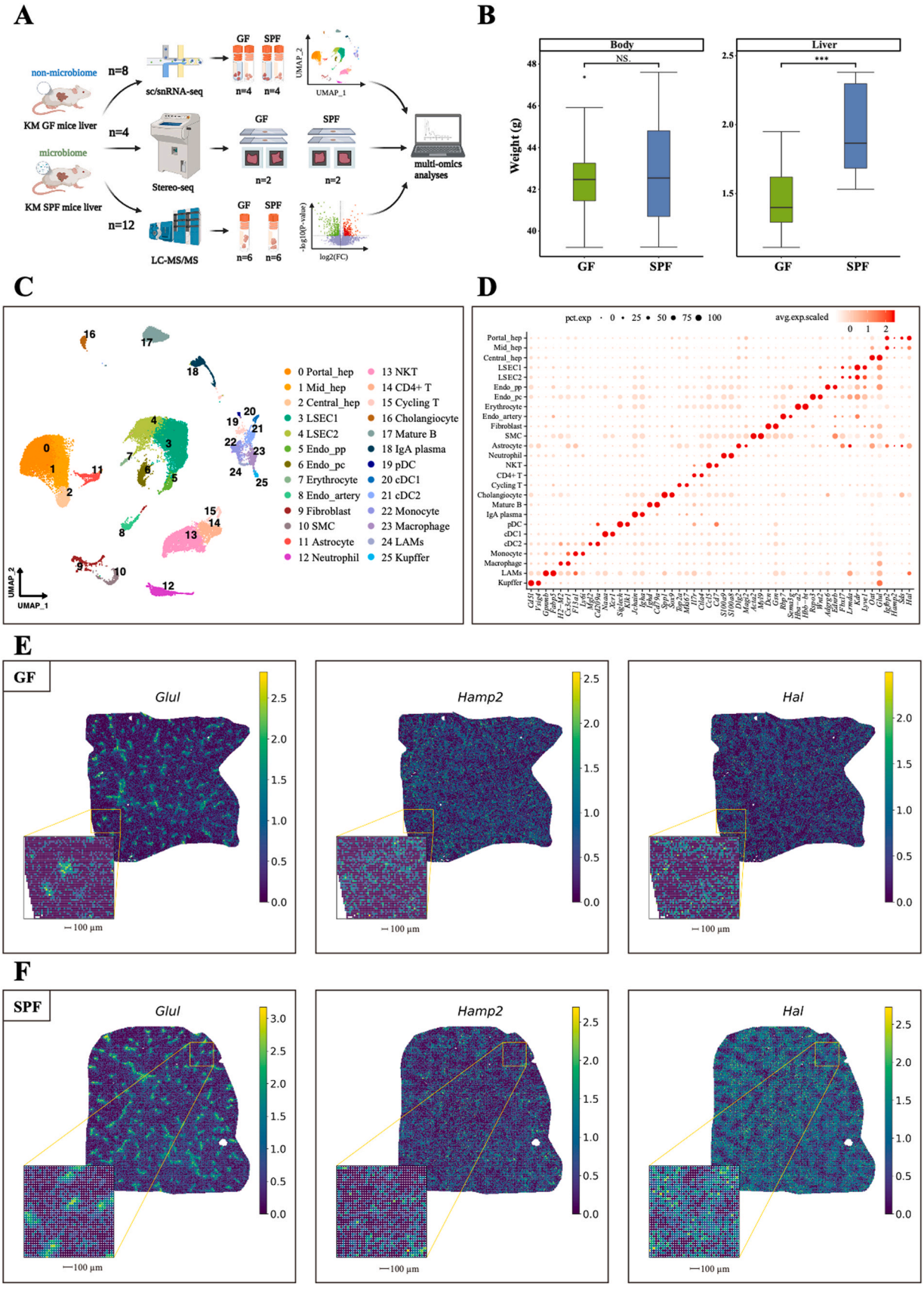

Fig. 1. Landscape of the article. **A:** Diagram showing the experimental design of this study. **B:** The left box plots show the statistical results of the body weights of GF and SPF mice (n = 14). The right box plots indicate the difference in liver weights between GF and SPF mice (n = 11). **C:** UMAP plot showing the 26 clusters of major cell types identified using the Seurat R pipeline. Cell type annotation for all major clusters is provided in the legend to the right. **D:** Dot plot illustrating cluster-specific gene expression. The normalized average UMI values for each cluster are represented by the dot size and colour intensity. **E, F:** Projection of selected marker genes for central venous expression (*Glul*, left), mid layer expression (*Hamp2*, middle), and periportal expression (*Hal*, right) in spots from the GF (E) and SPF (F) mouse liver tissues.

that the innate lymphoid cells of the intestine originate from the foetal liver [26,42]. Related investigations also suggest that the mature liver and intestine communicate bidirectionally around the bile ducts, portal vein, and body circulation, and this bidirectional communication mechanism is critical in developing and progressing liver disease [57]. More importantly, microorganisms and their metabolites play an important role in the enterohepatic cycle. Intestinal and hepatic communication mediators are mainly derived from the intestinal blood, which contains a variety of bacterial metabolites and endotoxins that enter the liver via the portal vein [4]. In addition, microorganisms can shape the immune system and play an essential role in glucose and lipid metabolism in the body by regulating the synthesis of bile acids [13,54].

In recent years, the development of GF mice has incredibly enhanced research on the gut-liver axis [14,35,8]. Histomorphological studies have revealed that the caecum of GF mice is enlarged 4–8 times due to the accumulation of mucus and undigested fibres, but the liver is reduced in size [3]. Functional studies have shown that D-lactic acid produced by intestinal flora metabolism can reach the liver directly through the portal vein, altering the morphology and size of hepatic Kupffer cells and enhancing the catching and killing of pathogens [41]. More interestingly, a recent study of GF and SPF mice revealed that the periportal region of the hepatic lobules is enriched in myeloid cells (such as hepatic macrophages) and lymphocytes (such as NKT cells), forming an immune compartmentalization phenomenon that facilitates defence against the spread of a blood-borne pathogen (Gola et al., 2021). Moreover, the intestinal microbiota is also considered a metabolic organ, which produces many metabolites (such as short-chain fatty acids, bile acids, and indole derivatives) that signal through their cognate receptors to regulate the metabolism of the host [59]. It has been demonstrated that hepatocytes can be divided into two different groups based on metabolic zonation [30,37], one around the hepatic central vein and another around the hepatic portal vein, and that genes in the liver lobules are also zonally expressed [49]. However, adequate technical methods for obtaining high-resolution spatial functional profiles still need to be improved, and the specific effects of the intestinal flora on liver metabolism still need to be discovered.

To meet these limitations, we urgently need new and comprehensive histological techniques have can further describe and correlate the gut-liver axis at the spatial, cellular, functional, and molecular levels. GF mice have no flora and act as a convenient animal model for the study of enterohepatic circulation. Previous studies have shown a clear gut-liver axis between GF and SPF mice [14,35,8], but the molecular characteristics and mechanisms of these differences are unclear. In recent years, scRNA-seq technologies have undergone rapid development. In July 2019, human liver cells were successfully mapped, and the results revealed new subtypes of hepatocytes, endothelial cells, and Kupffer cells that had never been previously described [2]. Although high-throughput sequencing and analysis at the single-cell level can address cell heterogeneity and discover new cell types, information on the spatial location of cells is lost [38]. The new ST sequencing technology, Stereo-seq [12], which can achieve subcellular-level resolution and a field of view of 1 cm * 1 cm as well as high sensitivity and a uniform capture rate, is expected to address these issues. Therefore, we used multiomics techniques to investigate the role of microorganisms in liver immunity and metabolism at the spatial, cellular, and molecular levels. The addition of ST captures the expression of all genes in the section, allowing the precise localization of gene expression levels at each layer and establishing a foundation for more detailed liver zonation studies.

2. Results

2.1. Single-nucleus/cell and spatial transcriptomic atlas of the GF and SPF mouse livers

A protocol has been designed to study the effect of microorganisms on liver phenotype and function. This study focused on sc/snRNA-seq, Stereo-seq, and metabolomics sequencing using livers from GF and SPF mice (Fig. 1A). First, the body weights of GF and SPF mice (n = 14, respectively) were measured. After sacrifice, the livers (n = 11) were removed and weighed. We discovered no significant difference in body weight between the GF and SPF mice. In contrast, the liver weights of GF mice were significantly lower than those of SPF mice (p value < 0.01, Fig. 1B), as reported previously [3].

Second, to investigate the effect of microbes on the liver at the cellular level, we used a combination of single-cell and single-nucleus RNA sequencing techniques. Fresh GF (pools of three biological repeats) and SPF (pools of three biological repeats) mouse livers were profiled by scRNA-seq, and frozen GF (n = 1) and SPF (n = 1) mouse livers were profiled by snRNA-seq. All experiments used the DNBelab C4 system for library generation. The scRNA-seq data were filtered based on an average gene expression per cell of 1397 and 1260 in GF and SPF mice, respectively (Fig. S1A, left). By integrating the filtered snRNA-seq data from cells identified as hepatocytes, we retained transcriptome data for a total of 36,533 cells/nuclei, with 14,586 and 21,947 cells/nuclei and an average gene expression of 1113 and 1255 in GF and SPF mice, respectively (Fig. S1A, right). After integration, the UMAP plot (Fig. S1B) and correlation analysis (Fig. S1C) of both the GF and SPF mice showed highly significant correlations between the samples. The UMAP plot after clustering is shown in Fig. 1C, and 26 cell types were obtained by annotation. This plot contains three types of hepatocytes, including the periportal hepatocytes (Portal_hep), middle hepatocytes (Mid_hep) and pericentral hepatocytes (Central_hep); five liver sinusoidal endothelial cells (LSEC), namely, LSEC1, LSEC2, periportal (Endo-pp) and pericentral endothelial cells (Endo-pc) [63] and artery endothelial cells (Endo-artery); five types of lymphoid cells, namely, natural killer T cells (NKT), $CD4^+$ T cells, cycling T cells, mature B cells (Mature B) and IgA plasma cells; eight types of myeloid cells, namely, neutrophils, plasmacytoid dendritic cells (pDC), two subsets conventional DCs (cDC1 and cDC2), monocytes, macrophages, lipid-associated macrophages (LAMs) and Kupffer cells. All cell types were defined according to their marker genes (Fig. 1D; Table S1): cDC1s mainly express *Xcr1* and *Naaa*, and cDC2s mainly express *Mgl2* and *Cd209a*; LAMs are characterized by *Gpnmb* and *Fabp5* [27]; Kupffer cells are identified by genes such as *Cd5l* and *Vsig4*; and macrophages are determined according to *H2 −M2* and *Cx3cr1* expression.

Third, to determine the spatial location of all mRNAs in the sections, we performed separate Stereo-seq [12] of the livers of GF (n = 2) and SPF (n = 2) mice. One of the high-quality groups makes up the primary dataset, whereas the other acts as a proof sample. The ST results (bin 50) of GF mice consist of 81,039 spots on the array with 22,956 genes, and those of SPF mice consist of 65,165 spots with 23,230 genes. The spots were filtered using a minimum expression threshold of 500 genes, and those with a mitochondrial proportion greater than 2% were eliminated. The remaining GF and SPF samples contained 80,843 and 64,995 spots, respectively, with 18,962 and 19,244 genes. The average gene expression levels in each spot of the GF and SPF samples were 891 and 1114, respectively (Fig. S1D), allowing us to produce a liver ST atlas that was evenly captured and of extremely high quality (Fig. S1E, top). The proof group had slightly worse capture (Fig. S1E, bottom) than the primary group and was only used to confirm the differences in gene expression between the GF and SPF mice. Using spatial transcriptome experiments, we obtained information about the location of all cells and gene expression in liver sections. Different spatial locations of the liver lobules perform various functions, and the lobules can be traditionally divided into three zones [30]. Marker genes of the three zones were selected and mapped on the ST data (Fig. 1E and Fig. 1F). *Glul* represents pericentral hepatocytes, *Hamp2* represents middle hepatocytes, and *Hal* represents periportal hepatocytes. Our dataset yielded a high-resolution spatial transcriptome atlas and a single-nucleus/cell transcriptome atlas of the GF and SPF mouse livers, providing a new resource for further dissecting the liver structure and function.

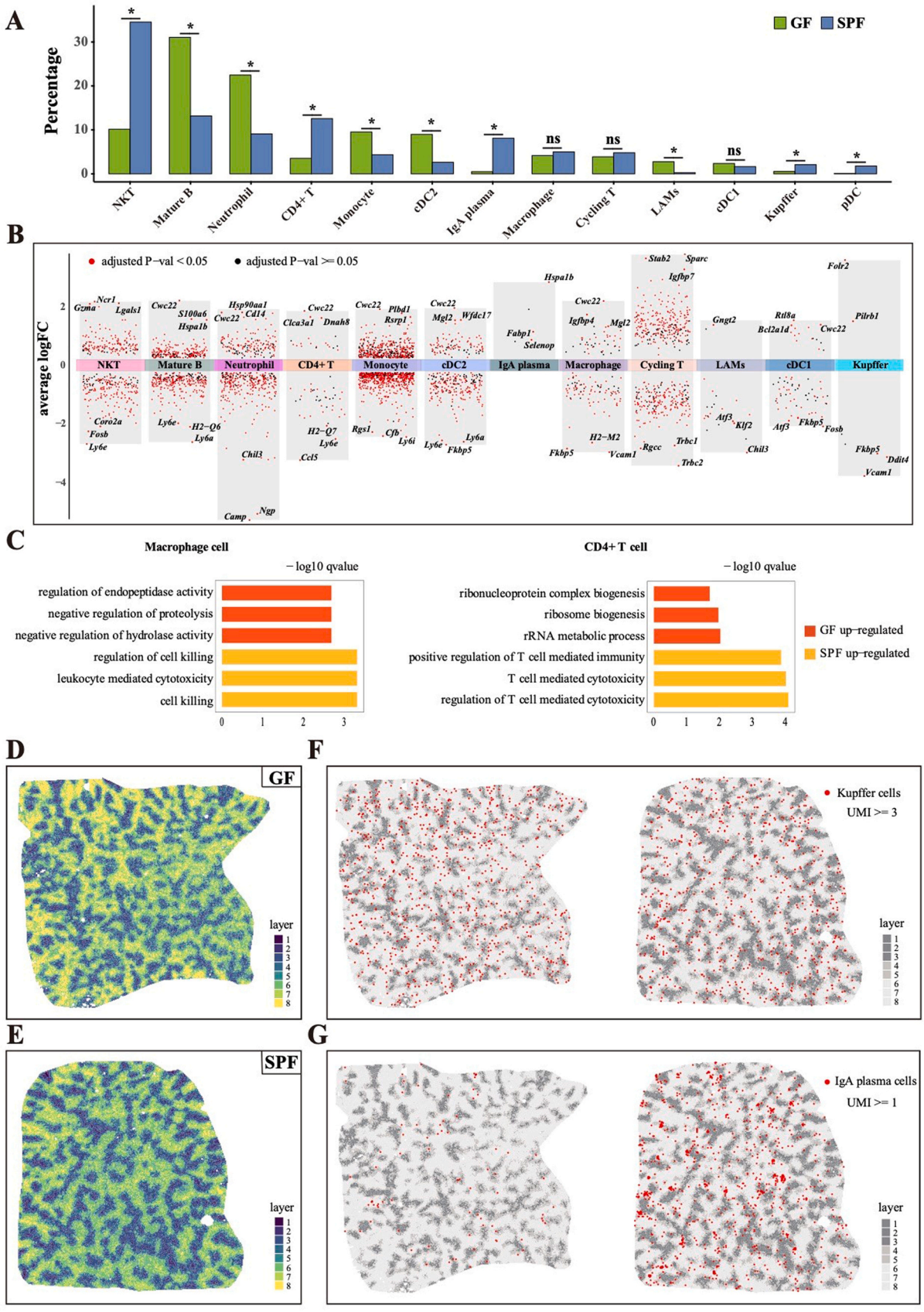

Fig. 2. Differences in hepatic immune cells between GF and SPF mice. **A**: Percentage of GF (green) and SPF (blue) mouse liver immune cells in each cluster. **B:** DEG map for each cell type, with the top half representing genes that were highly expressed in GF mice and the bottom half representing genes that were highly expressed in SPF mice. **C:** GO annotations showing the main functions of macrophages (left) and CD4$^+$ T cells (right) in GF and SPF mouse livers based on their DEG profiles. The bar plot displays three terms of each group. **D, E:** Visualization of hepatic lobule layers based on the ST data of the GF (**D**) and SPF (**E**) mouse livers. **F, G:** Visualization of the expression of markers of Kupffer cells (*Cd5l* and *Vsig4*) (**F**) and IgA plasma cells (*Jchain* and *Igha*) (**G**) in spots of GF (left) and SPF (right) tissue sections.

2.2. Microbes affect the function and ecological niche of hepatic immune cells

Next, we further analysed the differences in immune cells between GF and SPF mice. First, the analysis of the percentages of the different immune cell types from the sc/snRNA-seq data showed that some immune cells, such as NKT cells, CD4 + T cells, and IgA plasma cells, were significantly decreased in GF mice compared to SPF mice (p value < 0.01, Fig. 2A). Reportedly, the number of $CD4^+$ T cells and plasma cells in the lamina propria of the intestine of GF mice was reduced, and IgA production was decreased, leading to further impairment of intestinal barrier function [21]. This finding suggests that the immune function of the liver of our GF mice may also be impaired due to the close communication between the gut and liver axis. Therefore, it can be concluded that microorganisms may influence their function by altering the cellular ratio.

Second, to analyse the differences among each cell type, we identified the differentially expressed genes (DEGs) for all immune cells using sc/snRNA-seq data (Table S2). The pDC cell type was excluded from the analysis due to the lack of cell numbers from GF mice. The results showed that the *Vcam1* gene was significantly more highly expressed in both macrophages and Kupffer cells in SPF mice than in GF mice (Fig. 2B), and this gene was associated with immune function. Lipopolysaccharide (LPS) has been reported to cause a significant increase in *VCAM-1* expression in Kupffer cells, which may promote leukocyte influx and play a role in tissue injury during infectious shock [58]. In the $CD4^+$ T cell population, *Ly6e* expression is high in SPF mice and lower in GF mice (Fig. 2B). The major functions of *Ly6e* are related to immunomodulation, particularly the regulation of T-cell activation, proliferation, and development [32,39,46,51]. To better understand the function of immune cells, we performed GO enrichment analysis of DEGs between GF and SPF mice. We found that the function of macrophages in SPF mice is mainly cell killing and immune cell-mediated cell death, whereas the function of those in GF mice is to regulate endopeptidase and hydrolase activity (Fig. 2C, left). This finding is consistent with a previous study showing that GF mice may have less efficient immune function [41]. A similar phenomenon is observed not only for macrophages but also for $CD4^+$ T cells. The main functions of $CD4^+$ T cells in SPF mice are enriched for activating T cells and regulating the adaptive immune response, whereas these functions are not significant in GF mice (Fig. 2C, right). Thus, microbes may influence the process of immune cells by regulating their expression of critical genes.

Third, to explore the effect of microbes on the spatial distribution of immune cells, we combined the Stereo-seq data with the liver zonation algorithm published in Nature [29], which allowed us to accurately divide the liver lobules into eight layers (Fig. 2D and Fig. 2E), with layer 1 representing the pericentral region and layer 8 representing the periportal region. To facilitate the observation, we grouped the layers into three zones. We defined layers 1–3 as the pericentral zone, layers 4–5 as the intermediate zone, and layers 6–8 as the periportal zone by calculating the percentage of each zone in the liver lobules [6], and each zone was displayed in the same colour. The mapping of Kupffer cell markers (*Cd5l* and *Vsig4*) on three zones showed that immune cells such as Kupffer cells were more aggregated around the periportal in SPF mice (Fig. 2F). Similar results were obtained using other markers (Fig. S2A), supporting the findings of previous authors [25]. This finding further indicates that SPF mice are more resistant to pathogen entry into the host than GF mice. Furthermore, by mapping IgA plasma cell markers (*Jchain* and *Igha*) on the three zones of the ST results, we observed that the number of markers was significantly higher in SPF mice than in GF mice, indicating an aggregated distribution in the portal vein (Fig. 2G and Fig. S2B). Liver IgAs have been reported to clear gut-derived antigens reaching other organs via portal circulation, protecting them from pathogens [44]. Taken together, the results indicate that microorganisms can influence immune cell proportions, gene expression, and spatial distribution.

Fourth, to investigate the effect of microbes on signalling between immune cells, we performed CellChat and single-cell regulatory network inference and clustering (SCENIC) analyses of the sc/snRNA-seq data. The CellChat results showed that the number and strength of cell–cell interactions were stronger in SPF mice than in GF mice (Fig. S2C and Fig. S2D). Interestingly, 40 out of 59 pathways were highly active in both GF and SPF livers, albeit at different levels (Fig. S2E). These likely represent core pathways that are necessary for liver function regardless of the microbiome (i.e., GF vs. SPF). Eleven pathways are active only in GF mice, and these include pathways important for angiogenesis processes such as ESAM [33,47] and VEGF [22]. Eight pathways are specifically active in SPF mice, and these include known immune regulators such as CD6 [11,53] and IL16 [23]. Both MHC- I and MHC- II were significantly decreased in GF mice, which suggests that GF mice may have an immune defect [15,40,50]. In addition, CXCL was lower in GF mice, and it has been reported that the phenomenon of Kupffer cell aggregation to the periportal vein is driven by the chemokine CXCL9 [24], further demonstrating the weaker immune function of GF mice. The SCENIC analysis of sc/snRNA-seq immune data also revealed significant differences between GF and SPF mice (Fig. S2F). Each cluster of immune cell types has its own specific set of activated transcription factors and differs significantly between GF and SPF mice. For example, *Mafb*(+) and *Spic*(+) regulators are highly enriched in SPF Kupffer cells. Conversely, *Etv1*(+) and *Hes1*(+) are highly enriched in GF Kupffer cells. The transcription factor *Mafb*(+) can promote specific Kupffer cell differentiation [52]. In conclusion, microbes can also have an impact on the function of immune cells by altering their cell–cell interactions and transcription factors.

2.3. Microorganisms mediate gene expression levels and metabolism in hepatocytes

To further investigate the effect of microorganisms on the function of different layers of hepatocytes, the ST data of GF and SPF mice were then deconvoluted using a published single-cell dataset [45] to resolve the cellular components of each spot in the ST data. The single-cell dataset has ten cell types containing four types of liver parenchymal cells, B cells, T cells, cholangiocytes, endothelial cells, stellate cells, and macrophages. The deconvolution results were visualized using the SPOTlight method with the maximum fraction of each spot (Fig. 3A). Next, we wanted to investigate whether there were functional differences in the different liver lobule layers between GF and SPF mice. Because fewer mid-portal hepatocytes were observed, the midcentral hepatocytes were combined with the mid-portal hepatocytes to yield an intermediate layer. The enrichment results revealed slight differences between the layers within the groups but significant differences between the groups, and the fatty acid metabolic processes differed significantly between GF and SPF mice and between the layers of the liver lobules (Fig. 3B). Similar results were obtained using the results of algorithmic layering to perform the same analysis (Fig. S3A).

To demonstrate that microorganisms also have an effect on fatty acid-related metabolites, we performed untargeted metabolic sequencing (n = 12) of the liver. Numerous metabolites were found in untargeted metabolomic reports (Table S3 and Table S4), and the 3-(2-hydroxyphenyl) propionic acid content was significantly higher in SPF mice than in GF mice (p value = 0.032, Fig. 3C). After absorption through the colon, propionate enters the liver through the portal vein. This metabolite is metabolized by hepatocytes, participating in the reversal of pyruvate to glucose [28] and lowering the blood low-density lipoprotein (LDL) and cholesterol levels, which was consistent with our biochemical blood results (Table 1). Based on a

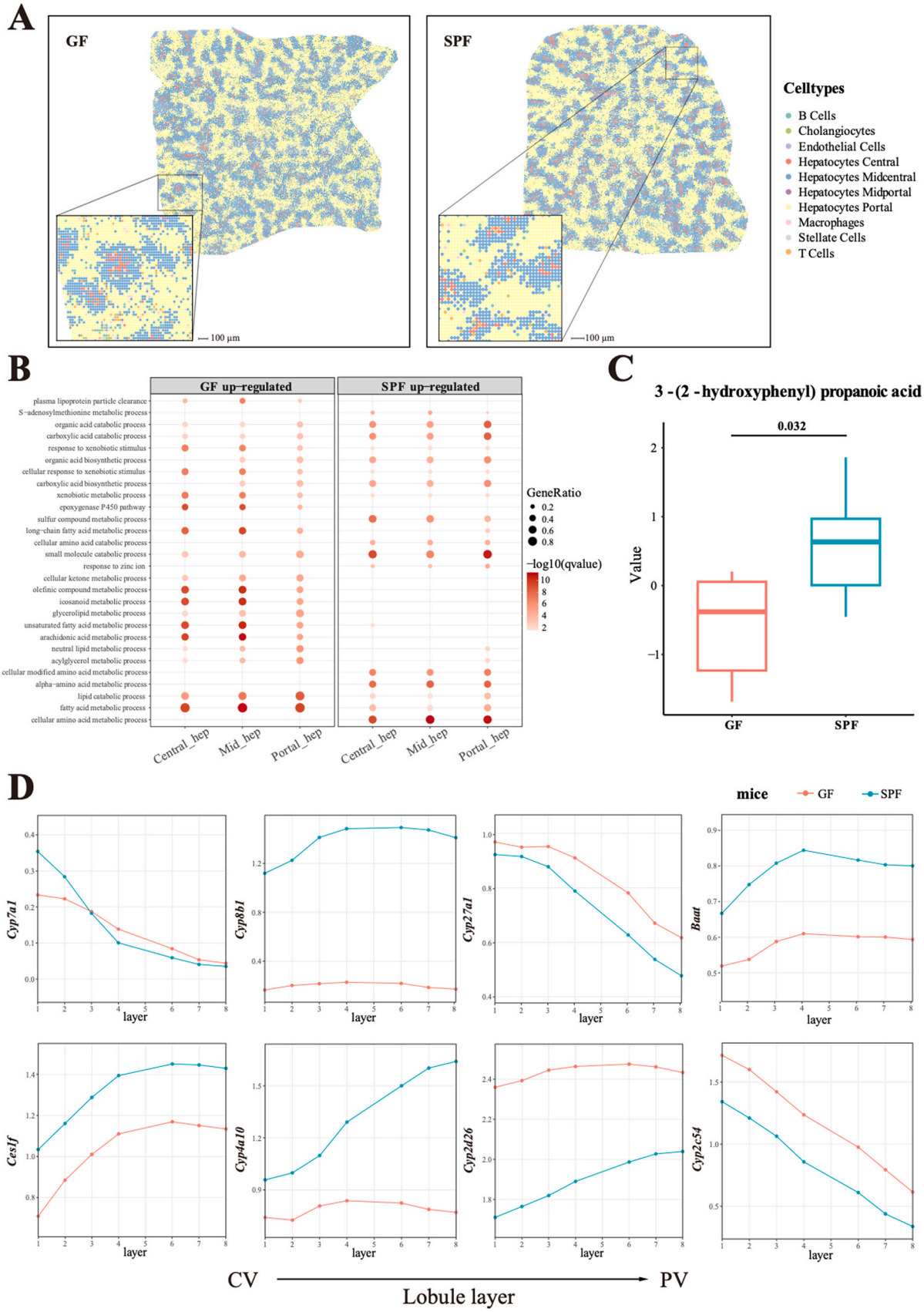

Fig. 3. Influence of microorganisms on the metabolic zonation of the liver. A: The spatial scatter plot represents the maximum proportion of cells in the reference atlas that capture locations in the livers of GF and SPF mice; we can observe the substructure of the lobular regions of the liver defined by their specific cell types. **B:** Enriched GO terms for the DEGs of GF and SPF mice in each liver layer. **C:** The content of propionic acid in the liver of GF (red) and SPF (blue) mice; the data were scaled. **D:** The spatial order of genes in GF (red) and SPF (blue) mice is consistent with their position in the classical bile acid biosynthesis cascade but with different expression levels. Layers 1–8 represent the direction of CV to PV. CV, central vein; PV, portal vein.

Table 1
Blood biochemistry test.

Name	GF/n	Mean ± SD	SPF/n	Mean ± SD	P value	Enriched
TG (mmol/L)	11	1.18 ± 0.62	9	1.55 ± 0.73	0.234	SPF
CHO (mmol/L)	11	3.25 ± 0.65	9	3.76 ± 0.86	0.154	SPF
HDL (mmol/L)	11	1.99 ± 0.28	7	2.50 ± 0.44	0.009	SPF
LDL (mmol/L)	11	0.40 ± 0.18	7	0.26 ± 0.06	0.04	GF

Table 1. TG, triglyceride; CHO, cholesterol; HDL, high-density lipoprotein; LDL, low-density lipoprotein.

previous study, propionic acid can affect the cholesterol levels and lipid metabolic processes [56].

Furthermore, to investigate the microbial effects on bile acid and fatty acid metabolism at the gene level, we used ST data to characterize the expression levels and distribution of genes. First, we used ST data to visualize critical genes for bile acid cascade synthesis (Fig. 3D, top). The overall trend of these genes in GF and SPF mice was more consistent with previous reports [17]. However, *Cyp8b1* gene expression was markedly downregulated in GF mice, and this phenomenon was also observed with the proof ST samples (Fig. S3B) and was in conformity with the results of other studies [36]. In addition, immunofluorescence staining results showed that CYP8B1 was significantly reduced in the GF group (Fig. S3C). This finding suggests that microorganisms may be involved in the process of bile acid synthesis. Next, focusing on the effect of microbes on the fatty acid metabolic process, we discovered that GF mice metabolize unsaturated fatty acids and long-chain fatty acids mainly in the central and intermediate layers (Fig. 3B and Fig. S3A). Short-chain fatty acid metabolism-related genes (*Ces1f*) are primarily enriched in the periportal vein, and long-chain fatty acid-related genes (*Cyp2c54*) are highly expressed mainly in the central periportal vein. In addition, the expression of genes metabolizing short-chain fatty acids was higher in SPF mice, whereas the expression of genes metabolizing long-chain fatty acids was higher in GF mice (Fig. 3D, bottom). For medium-chain fatty acids, lauric acid, a saturated fatty acid, is predominantly metabolized in SPF (*Cyp4a10*). However, arachidonic acid, an ω-6 polyunsaturated fatty acid widely found in cell membranes, is predominantly metabolized in GF mice (*Cyp2d26*). Unsaturated fatty acids promote high-density lipoprotein (HDL) synthesis, which is beneficial to vascular health. In contrast, saturated fatty acids are more likely to encourage the synthesis of LDL; thus, GF mice have lower HDL (P value = 0.009) and higher LDL levels (P value = 0.04, Table 1). Fatty acid metabolism-related genes were also differentially expressed between GF and SPF mice (Fig. S3D). These results demonstrate that microorganisms possibly affect liver metabolic function by altering gene expression and distribution, metabolic pathways, and metabolites.

2.4. Microorganisms impact the zonation patterns and functions

To investigate which gene zonation patterns are controlled by microbes, we calculated the average expression of all genes in each layer of the liver lobules using linear and nonlinear fits; specifically, the genes which were divided into three patterns based on their expression trends: genes that were highly expressed in the pericentral layer, genes that were highly expressed in the intermediate layer, and genes that were highly expressed in the periportal layer. According to these patterns, all genes with the same expression level in GF and SPF mice were identified. The analysis identified 347 genes with high expression in the pericentral vein, 411 genes with elevated expression in the intermediate layer, and 333 genes with increased expression in the periportal vein of both GF and SPF mice, and three genes are shown in the figure (Fig. 4A; Table S5-S7). Then, genes with inconsistent expression patterns between GF and SPF mice were discovered (Table S8-S10). In SPF mice, 429, 436 and 148 genes were significantly more highly expressed around the central vein (Fig. 4B, left), the middle layer (Fig. 4B, middle), and the portal vein (Fig. 4B, right), respectively, whereas these genes did not exhibit the same significant pattern in GF mice. Thus, microorganisms may regulate the expression of genes between different layers of the liver lobules.

To further understand the functions influenced by the enriched expression of genes in different regions, two categories were defined regarding whether the region was affected by zonation enrichment. First, we conducted GO enrichment analyses of genes with consistent expression patterns between GF and SPF mice and identified the pathways enriched in the pericentral zone, intermediate, and periportal zone (from top to bottom, Fig. S4A, left). The critical genes in one of the pathways were then selected separately for display (Fig. S4A, right). We found significant differences in the expression levels of genes related to arginine biosynthesis in GF and SPF mice (Fig. S4B), whereas all these genes were highly expressed in the periportal zone. This result indicates that microbes may regulate the expression of metabolism-related genes without altering their expression patterns. Second, we performed functional enrichment analyses of genes showing different expression patterns between GF and SPF mice. From top to bottom, Fig. 4C displays the results of the enrichment analysis for the genes in Fig. 4B (Fig. 4C, left). Our results also showed that, consistent with previous findings, the lipid biosynthetic process in SPF mice was mainly enriched in the pericentral vein [16], and fatty acid beta-oxidation was primarily enriched in the periportal vein [7]; however, in GF mice, the findings were clearly different. Microbial alterations in lipid metabolism may be responsible for a reduced liver weight [64]. Genes classified as showing one of the three patterns were selected separately for display (Fig. 4C, right). For example, the lipid biosynthetic process is highly expressed in the pericentral vein in SPF mice with a decreasing trend, whereas in GF mice, the corresponding genes are mainly highly expressed in the intermediate layer. Genes with class I MHC-mediated antigen processing and presentation functions are most highly expressed in the middle layer in SPF mice, whereas in GF mice, the related genes are most highly expressed in the pericentral vein. The critical genes of the fatty acid beta-oxidation process were highly expressed in the periportal vein of SPF mice, whereas in GF mice, the related genes were mainly enriched in the central and intermediate layers. Genes related to the fatty acid beta-oxidation process were all significantly more highly expressed in SPF mice (Fig. S4C), demonstrating that microorganisms affect the distribution of their expression in the liver. The evolutionary conservation of many MHC class Ib molecules suggests that unconventional T cells may play an important role in host physiology, particularly in mediating interactions with the microbiota and maintaining tissue homeostasis [15]. Thus, microorganisms may affect liver immune and metabolic functions by altering gene expression levels or tendencies in liver lobules.

3. Discussion

Our study combined single-nucleus/cell RNA sequencing with ST techniques to reconstruct a cellular atlas of GF and SPF mouse livers. Furthermore, the microbial effects on the mouse liver are also analysed at multiple levels, including cellular, genetic, spatial distribution, and metabolite levels. Previously, ST technology could not reach the single-cell level due to technical hindrances; thus, combining ST data with single-cell and other omnidirectional data from the same

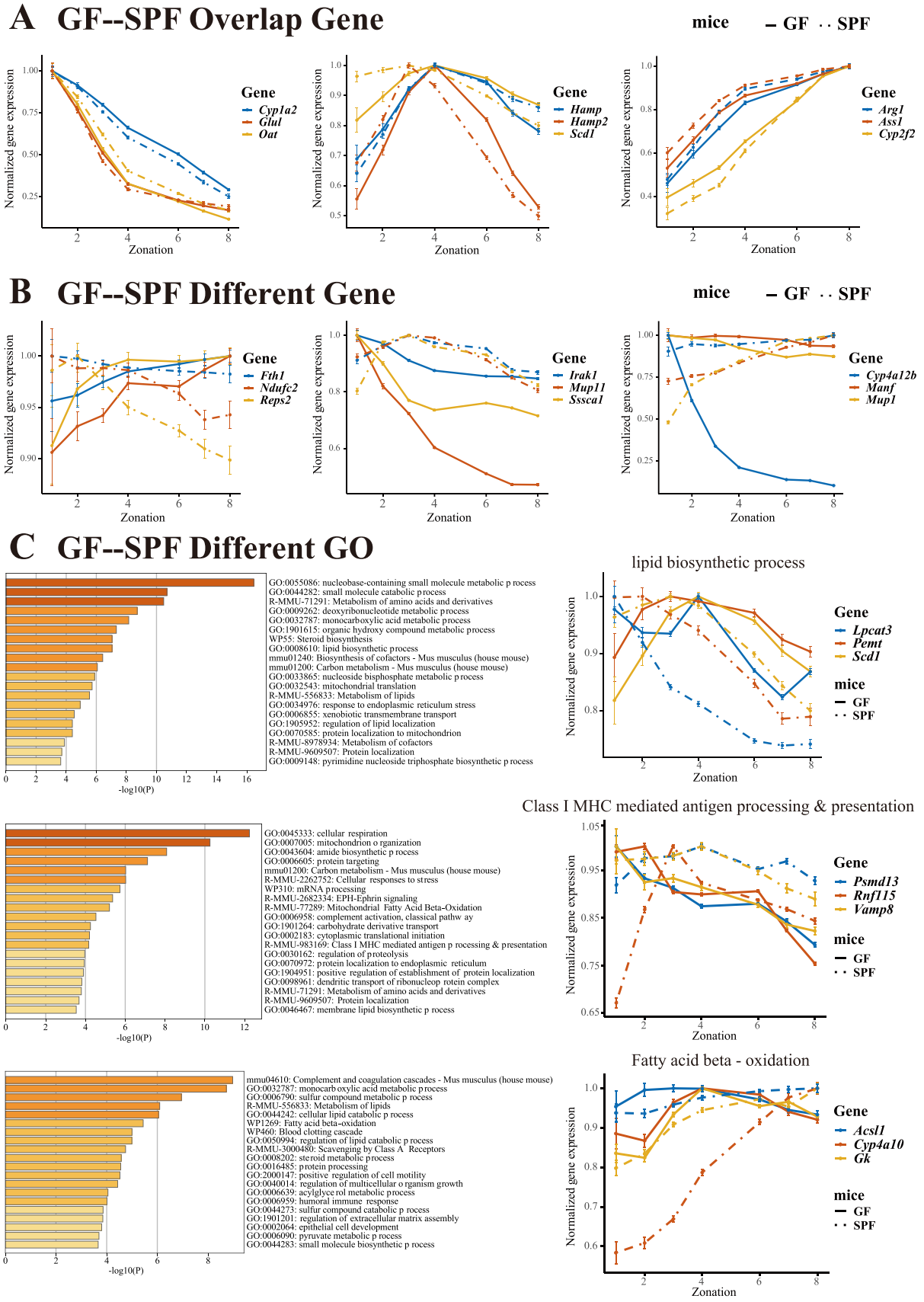

Fig. 4. Microorganisms can affect the gene expression patterns in liver lobules. **A**: Three patterns of similar gene expression trends in GF and SPF mouse livers. **B:** Three patterns of differential gene expression trends in GF and SPF mouse livers. **C:** Metascape was used to analyse the functional enrichment of genes with different expression patterns in GF and SPF mice according to the three categories in (B) (left), and the line graph (right) indicates the distribution of gene expression levels with one of the functions corresponding to those on the left on the liver lobules. The solid line represents GF mice, and the dashed line represents SPF mice. Three genes for each pattern are shown to make it more obvious.

tissue was necessary [43,48] in this study. Moreover, with the development of ST technologies, the accuracy can reach the subcellular level, providing an unprecedented level of insight into the biology of tissues.

First, Kupffer cells in the periportal vein can resist the spread of pathogens in the blood, and the formation of this zonation is driven by bacteria [25]. Our results showed that Kupffer cells were more enriched towards the periportal region in SPF mice than in GF mice (Fig. 2F and Fig. S2A). These findings provide initial support for the significance of the previously proposed immune zonation [25]. The liver is constantly threatened by toxicity and microorganisms from the periportal blood. GF mice may be less effective immunologically because they are not affected by microorganisms, as could be suggested by the functional enrichment of Kupffer cells and $CD4^+$ T cells. Therefore, it will be essential to perform ST to study the effect of microorganisms on immune zonation.

Second, liver metabolism was additionally examined. To ensure that differences in metabolites were not influenced by diet, all control mice were fed a uniform diet. This part of the study focused on the differences in propionate between the livers of GF and SPF mice. Using combined metabolomic and spatial data, we obtained some metabolic pathway partitioning regulated by microorganisms in addition to validating the previously mentioned hepatic metabolic zonation [7,9], which provided some evidence for further hepatic metabolic zonation studies. Nevertheless, the specific molecular mechanisms of metabolites affecting partitioning need to be solved.

Furthermore, the ST data generated in this study support the hypothesis that the primary source of spatial heterogeneity throughout the liver tissue is transcriptional differences between the portal and central veins along the lobular axis region [29,30]. This study demonstrates that genes differ along the axes of the liver lobules and that microorganisms may alter the expression of some genes along the lobule axes. However, some gene expression fits may not be very precise due to the broad linear and nonlinear fitting restrictions, but it is possible to determine the overall trend. Different layers of the lobular microenvironment give rise to different spatial partitioning of hepatocytes [29,30,5]. This study can provide a reference for the subsequent microbial changes in the function of hepatocytes on the lobules.

There is still much to learn regarding the functional basis of the interlobular liver and how the organ maintains its structural integrity. Considering the sample size used in this study, we can provide preliminary indications rather than general claims about the function of this structure. In addition to capturing and supporting previously observed trends in tissue heterogeneity in the mammalian liver, our study may serve as a valuable resource to further investigate the structural components and spatial expression of candidate genes involved in the above processes and to identify some novel trends. By including GF mice, it is also possible to determine which trends may be influenced by the colony.

Increasing the resolution and capture rates of ST will enable detailed investigation of novel cellular subtypes within tissues [62]. At the same time, 3D reconstructions will provide a more comprehensive view of the tissue structure [60], which would significantly aid the identification of changes in tissue subregions and cellular states. This study explored the potential benefits of ST in liver research and demonstrated the spatial distribution of genes in the GF mouse liver as a precious resource for hepatology research. The spatial transcriptome may also have significant implications for future liver development, immunity, metabolism, and pathology studies.

4. Methods

4.1. Mice

A total of twenty-eight 10-week-old male Kunming (KM) mice were procured from the Experimental Animal Center of Huazhong Agricultural University (Wuhan, China), and these consisted of fourteen germ-free (GF) mice and fourteen specific-pathogen-free (SPF) mice. The mice were housed in a pathogen-free colony (temperature, 25 ± 2 °C; relative humidity, 45–60%; lighting cycle, 12 h/day; light hours 06:30–18:30) with free access to food and water. The Institutional Animal Care and Use Committee of Huazhong Agricultural University, Hubei, China, approved all animal experiments and sample collection procedures. All experimental methods in this study were carried out following the Guide for the Care and Use of Laboratory Animals at Huazhong Agricultural University. The animal experiment ethics number for this study is BGI-IRB A21028.

4.2. Experimental design and sample collection

All mice were fed GF diets, which were produced according to our specially designed formula and sterilized by Co60-γ irradiation at 50 kGy to kill microorganisms [61]. Before being fed to the mice, the nutritional composition of the GF diets was tested according to standards. The body weight of each mouse at 10 weeks of age was measured before killing, and the mice were then euthanized by CO_2 inhalation followed by cervical dislocation to ensure death. Whole blood samples were collected from the orbital sinus of the mice. The mice were then dissected ventrally, and the entire liver was removed for weighing. First, a piece of the left lobe of the liver was cut for OCT embedding and used for ST experiments. Second, the liver was divided into 5 * 5 * 5-mm^3 segments and placed into lyophilization tubes using Miltenyi Tissue Preservation Solution for scRNA-seq research. Finally, for later detection of untargeted liver metabolites and snRNA-seq, small pieces of the liver from each animal were cut into lyophilized tubes, snap-frozen in liquid nitrogen for 15 min, and then promptly stored in a − 80 °C refrigerator.

4.3. scRNA-seq and snRNA-seq sample preparation and data filtering

Fresh liver tissues were sectioned into fragments to enable single-cell isolation, and these fragments were placed in RPMI-1640 medium (Invitrogen) supplemented with 1% penicillin-streptomycin (Pen-Strep). Subsequently, the tissue fragments were enzymatically digested using the Mouse MACS Liver Dissociation Kit (Miltenyi Biotec) at 37 °C for 30 min under agitation, following the manufacturer's instructions. The resulting dissociated cells were then passed through a 70-μm and 40-μm cell strainer (BD) and centrifuged at 300g for 10 min. After removal of the supernatant, the cell pellet was resuspended in red blood cell lysis buffer (Thermo Fisher) and incubated on ice for 2 min to induce lysis of red blood cells. Following two washes with PBS (Invitrogen), the cell pellet was resuspended in PBS containing 0.04% BSA. The frozen liver fragments were used for single-nucleus isolation performed via a mechanical separation protocol with a 2-mL Dounce apparatus (Sigma, D8938, USA), as described previously [31]. The DNBelab C Series Single-Cell Library Prep Set (MGI, 1000021082) was used to construct libraries, and the libraries were sequenced using a DNBSEQ-T7 sequencer at the China National GeneBank (Shenzhen, China). Raw sequencing reads were filtered and demultiplexed using PISA (v0.2; https://github.com/shiquan/PISA). The reads were aligned to the mouse reference genome (GRCm39) using STAR (v2.7.4a) [18] and sorted by sambamba (v0.7.0) [55]. Estimation of the ambient RNA contamination rate was conducted using SoupX [65] with the default settings. The cell preprocessing and filtering steps involved applying a minimal expression threshold of 200 genes and ensuring that genes were expressed in at least three cells. Only cells meeting these criteria were retained for subsequent analysis. Furthermore, cells with mitochondrial gene counts exceeding 15% were excluded. To identify and eliminate doublets, the default parameter of DoubletFinder was utilized, resulting in the removal of the 5% of cells displaying the highest similarity to pseudo-doublets. The nuclei

underwent preprocessing and filtering utilizing a minimal expression threshold of 500 genes for SPF samples and 200 genes for GF samples and a maximum threshold of 4000 genes. Subsequently, nuclei with mitochondrial gene counts surpassing 10% were excluded from the analysis.

4.4. Data integration and dimensional reduction

In adherence to the guidelines outlined by Seurat, we clustered and visualized the nuclei of GF and SPF mice separately using a standard workflow. The clusters annotated as hepatocytes were then individually selected and merged with their corresponding single-cell groups. The merged data were then subjected to debatching integration using the "FindIntegrationAnchor" and "IntegrateData" functions in Seurat [10]. Subsequently, data were normalized using the NormalizeData function with default options, and the top 2000 most variable genes of each replicate were then calculated by FindVariableFeatures with the vst method. PCA of the variable genes was performed using the RunPCA function in Seurat (version 4.3.0). The identities of clusters of cells were manually annotated using known marker genes in published articles with the help of the Mouse Cell Atlas database (https://bis.zju.edu.cn/MCA/) [20].

4.5. Stereo-seq experiments and data processing

The STOmics Gene Expression kit S1 (BGI, 1000028493) was utilized according to the standard protocol V1.1 [12]. The embedded samples were freeze-sliced to a thickness of 10 μm, adhered to the Stereo-seq chip, fixed by incubated in − 20 °C methanol for 30 min fixation, and then subjected to nucleic acid dye staining (Thermo Fisher, Q10212) and imaging (Ti-7 Nikon Eclipse microscope). The tissue was then permeabilized at 37 °C for 12 min and then subjected to reverse transcription, tissue removal, cDNA release, recovery, purification, and amplification. The cDNA was purified using AMPure XP beads (Vazyme, N411–03). Finally, libraries were sequenced using an MGI DNBSEQ-Tx sequencer (50 bp for read 1, 100 bp for read 2). The raw data were processed using the same procedure as in previous work (Chen et al., 2021). Clean reads were aligned to the mouse reference genome (GRCm39) using STAR [18]. Transcripts captured by 50*50 DNBs were merged as one bin 50. We treated bin 50 as the fundamental analysis unit. Bin IDs were synthesized by their spatial coordination (spatial_x and spatial_y) at the capture chip. Each chip bin has a diameter of approximately 220 nm and a centre-to-centre distance of 500 nm. Consequently, the centre distance of five bin 50 is approximately 100 μm.

4.6. Untargeted metabolomics

In this study, untargeted metabolomics analysis was conducted using LC−MS/MS technology. A high-resolution mass spectrometer Q Exactive HF (Thermo Fisher Scientific, USA) was used to collect data from both positive and negative ions. Compound Discoverer 3.3 (Thermo Fisher Scientific, USA) software was used to process the LC−MS/MS data, primarily for peak extraction, peak alignment, and compound identification. The result file from Compound Discoverer was inputted into the R package MetaX for data preprocessing and further analysis. For data dimensionalization, principal component analysis (PCA) was employed, with log transformation and Pareto scaling being the primary methods used to compute the principal components. Partial least squares-discriminant analysis (PLS-DA) was utilized to assess the significant differences between classification groups. Additionally, variable importance for projection (VIP) and Wilcoxon tests were used to identify and screen distinct metabolites.

4.7. Liver zonation

The ST data expression matrix was used as the first input. The probability of each spot in each layer was then calculated based on the prior chance of marker genes using MATLAB [29]. The layer in which the spot is located and visualized with the highest probability was then selected. This analysis yields a spatially displayed map of the distribution of liver lobules in layers 1–8. Referring to the literature on the ratio of three layers of liver lobules [6], we used layers 1–3, 4–5 and 6–8 of the ST data as the central venous region, intermediate region, and portal venous region, respectively.

4.8. DEGs and enrichment analysis

We used the FindMarkers function in Seurat to analyse DEGs among different cell types. DEGs were defined as genes with an absolute value of log2 fold change > 0.5 and adjusted P < 0.05. We then performed a Gene Ontology (GO) analysis of DEGs between each cluster in GF and SPF mice to illustrate the biological process and potential function of different cells using the clusterProfiler package (version 4.0.5) and org.Mm.eg.db package (version 3.13.0). Only GO terms with a Q value < 0.05 were retained (Fig. 2C). Genes with differential expression patterns were enriched for function (Fig. 4C and Fig. S4A) using the online site Metascape (https://metascape.org).

4.9. Cell−cell interaction

We used CellChat (version 1.6.0) [34] to assess cell interactions within each sample (GF and SPF mice). We created CellChat objects following the official CellChat workflow and used the mouse database of CellChatDB for subsequent analysis.

4.10. SCENIC analysis

SCENIC analysis [1] is a method for computational scRNA-seq data gene regulatory network reconstruction and cell state identification based on coexpression and motif analysis. SCENIC analysis involves the following three steps to complete the transcription factor analysis: the first step is to construct the coexpression network (GRNboost), the second step is to build the TF-target network (RcisTarget), and the third step is to calculate the regulon activity (AUCell). The input data are the single-cell gene expression matrix using the pySCENIC (version 0.11.2) and mm9–500 bp-upstream-7species databases for RcisTarget, GRNboost, and AUCell.

4.11. Deconvolution

We used the SPOTlight (version 1.0.1) method to integrate ST and scRNA-seq data to infer cell types and states within complex tissues. SPOTlight is centred around a seeded nonnegative matrix factorization (NMF) regression, initialized using cell-type marker genes and nonnegative least squares (NNLS) to subsequently deconvolute ST capture locations [19], and these locations were then used to determine the cell types and percentage at each spot.

4.12. Immunofluorescence staining

Tissue cryosections (8 μm) were washed with PBS and fixed in 100% methanol for 10 min at room temperature. After three washes with PBS, the tissue sections were blocked in blocking buffer (3% BSA, 0.3% Triton™ X-100 in PBS) for 30 min at room temperature and then incubated with primary antibody overnight at 4 °C. The next day, the tissue sections were washed with PBS and incubated with fluorescence-conjugated secondary antibodies for 1 h at room temperature. DAPI-containing mounting medium (Southern Biotech

#0100–20) was used to visualize the nuclei and preserve slides. The antibodies used were as follows: CYP8B1 (Affinity, DF4762; 1:200 dilution), Glutamine synthetase (BD Biosciences, #610517; 1:200 dilution), Cy3-conjugated Goat anti-rabbit IgG (Servicebio, GB21303; 1:200 dilution), and 488-conjugated Goat anti-mouse IgG (Servicebio, GB25301; 1:200 dilution). Images were acquired using a Nikon Eclipse C1 microscope and analysed using ImageJ software.

4.13. Linear and nonlinear models

To build a linear model (ax+b) of the mean gene expression with R, the intercept and slope terms were estimated using the lm function. The commonly used method is ordinary least squares (OLS) regression. If the P value (x) < 0.05 and coefficient (x) > 0.005, a significant monotonically increasing gene was considered highly expressed in the periportal vein; conversely, if the P value (x) < 0.05 and coefficient (x) < −0.005, a significant monotonically decreasing gene was highly expressed in the pericentral vein. The nonlinear model (ax^2 +bx+c) fits the genes highly expressed in the intermediate layer. The common method was nonlinear least squares (NLS) regression using the nls function with a P value of the coefficient of the quadratic term less than 0.05 and a coefficient of the quadratic term less than 0 (P value (x^2) < 0.05 and coefficient (x^2) < 0). The gene was highly expressed in the intermediate layer. The model was considered insignificant if the P value of the slope was more significant than 0.05.

CRediT authorship contribution statement

Ruizhen Zhao: Research protocol design, experiment follow-up, data analysis, drawing, writing, editing and literature source. **Wei Cheng, Hong Wei:** Breeding of model animals, literature source. **Zhao Zhang, Yifei Sheng, Weiming Liang:** Auxiliary data analysis. **Tailiang Chai, Xueting Chen, Yin Zhang:** Research protocol design, Sample collection, mouse dissection. **Juan Shen, Xiang Huang, Huanjie Yang:** Editing and correcting articles. **Li Pang,** Chunqing Song**, Cuoji Nan:** Experimental technical support. **Yangrui Zhang, Rouxi Chen, Junpu Mei:** Supervision. **Xiaodong Fang:** Coordinating the entire study, literature source.

Data availability

The sequencing data supporting the findings of this study have been deposited into CNSA (CNGB Sequence Archive) of CNGBdb (https://db.cngb.org/cnsa/): CNP0003996 and STT0000034.

Declaration of Competing Interest

The authors declared that they have no conflicts of interest to this work.

Acknowledgements

This research was made possible thanks to a grant from the Science Technology and Innovation Commission of Shenzhen Municipality, China (SGCX20190919142801722). The support of the China National GeneBank and the contributions of the authors are acknowledged. Fig. 1A was created with BioRender.com.

Appendix A. Supporting information

Supplementary data associated with this article can be found in the online version at doi:10.1016/j.csbj.2023.06.020.

References

[1] Aibar S, González-Blas CB, Moerman T, Huynh-Thu VA, Imrichova H, Hulselmans G, Rambow F, Marine J-C, Geurts P, Aerts J, et al. SCENIC: single-cell regulatory network inference and clustering. Nat Methods 2017;14:1083–6. https://doi.org/10.1038/nmeth.4463
[2] Aizarani N, Saviano A, Sagar, Mailly L, Durand S, Herman JS, Pessaux P, Baumert TF, Grün D. A human liver cell atlas reveals heterogeneity and epithelial progenitors. Nature 2019;572:199–204. https://doi.org/10.1038/s41586-019-1373-2
[3] Al-Asmakh M, Zadjali F. Use of germ-free animal models in microbiota-related research. J Microbiol Biotechnol 2015;25:1583–8. https://doi.org/10.4014/jmb.1501.01039
[4] Albillos A, de Gottardi A, Rescigno M. The gut-liver axis in liver disease: pathophysiological basis for therapy. J Hepatol 2020;72:558–77. https://doi.org/10.1016/j.jhep.2019.10.003
[5] Andersson A, Bergenstråhle J, Asp M, Bergenstråhle L, Jurek A, Fernández Navarro J, Lundeberg J. Single-cell and spatial transcriptomics enables probabilistic inference of cell type topography. Commun Biol 2020;3:565. https://doi.org/10.1038/s42003-020-01247-y
[6] Andrews TS, Atif J, Liu JC, Perciani CT, Ma X-Z, Thoeni C, Slyper M, Eraslan G, Segerstolpe A, Manuel J, et al. Single-cell, single-nucleus, and spatial RNA sequencing of the human liver identifies cholangiocyte and mesenchymal heterogeneity. Hepatol Commun 2022;6:821–40. https://doi.org/10.1002/hep4.1854
[7] Ben-Moshe S, Itzkovitz S. Spatial heterogeneity in the mammalian liver. Nat Rev Gastroenterol Hepatol 2019;16:395–410. https://doi.org/10.1038/s41575-019-0134-x
[8] Björkholm B, Bok CM, Lundin A, Rafter J, Hibberd ML, Pettersson S. Intestinal microbiota regulate xenobiotic metabolism in the liver. PLoS One 2009;4:e6958. https://doi.org/10.1371/journal.pone.0006958
[9] Braeuning A, Ittrich C, Köhle C, Hailfinger S, Bonin M, Buchmann A, Schwarz M. Differential gene expression in periportal and perivenous mouse hepatocytes. FEBS J 2006;273:5051–61.
[10] Butler A, Hoffman P, Smibert P, Papalexi E, Satija R. Integrating single-cell transcriptomic data across different conditions, technologies, and species. Nat Biotechnol 2018;36:411–20. https://doi.org/10.1038/nbt.4096
[11] Català C, Velasco-de Andrés M, Leyton-Pereira A, Casadó-Llombart S, Sáez Moya M, Gutiérrez-Cózar R, García-Luna J, Consuegra-Fernández M, Isamat M, Aranda F, et al. CD6 deficiency impairs early immune response to bacterial sepsis. iScience 2022;25:105078. https://doi.org/10.1016/j.isci.2022.105078
[12] Chen A, Liao S, Cheng M, Ma K, Wu L, Lai Y, Qiu X, Yang J, Xu J, Hao S, et al. Spatiotemporal transcriptomic atlas of mouse organogenesis using DNA nanoball-patterned arrays. Cell 2022:*185*. https://doi.org/10.1016/j.cell.2022.04.003
[13] Chiang JYL, Ferrell JM. Bile acid metabolism in liver pathobiology. Gene Expr 2018;18:71–87. https://doi.org/10.3727/105221618×15156018385515
[14] Claus SP, Tsang TM, Wang Y, Cloarec O, Skordi E, Martin F-P, Rezzi S, Ross A, Kochhar S, Holmes E, Nicholson JK. Systemic multicompartmental effects of the gut microbiome on mouse metabolic phenotypes. Mol Syst Biol 2008;4:219. https://doi.org/10.1038/msb.2008.56
[15] Constantinides MG, Belkaid Y. Early-life imprinting of unconventional T cells and tissue homeostasis. Sci *374*, eabf0095 2021. https://doi.org/10.1126/science.abf0095
[16] Cunningham RP, Porat-Shliom N. Liver Zonation - Revisiting Old Questions With New Technologies. Front Physiol 2021;12:732929. https://doi.org/10.3389/fphys.2021.732929
[17] de Aguiar Vallim TQ, Tarling EJ, Edwards PA. Pleiotropic roles of bile acids in metabolism. Cell Metab 2013;17:657–69. https://doi.org/10.1016/j.cmet.2013.03.013
[18] Dobin A, Davis CA, Schlesinger F, Drenkow J, Zaleski C, Jha S, Batut P, Chaisson M, Gingeras TR. STAR: ultrafast universal RNA-seq aligner. Bioinformatics 2013;29:15–21. https://doi.org/10.1093/bioinformatics/bts635
[19] Elosua-Bayes M, Nieto P, Mereu E, Gut I, Heyn H. SPOTlight: seeded NMF regression to deconvolute spatial transcriptomics spots with single-cell transcriptomes. Nucleic Acids Res 2021;49:e50. https://doi.org/10.1093/nar/gkab043
[20] Fei L, Chen H, Ma L, E W, Wang R, Fang X, Zhou Z, Sun H, Wang J, Jiang M, et al. Systematic identification of cell-fate regulatory programs using a single-cell atlas of mouse development. Nat Genet 2022;54:1051–61. https://doi.org/10.1038/s41588-022-01118-8
[21] Fessler J, Matson V, Gajewski TF. Exploring the emerging role of the microbiome in cancer immunotherapy. J Immunother Cancer 2019;7:1–15.
[22] Gerber H-P, Malik AK, Solar GP, Sherman D, Liang XH, Meng G, Hong K, Marsters JC, Ferrara N. VEGF regulates haematopoietic stem cell survival by an internal autocrine loop mechanism. Nature 2002;417:954–8.
[23] Ghigo E, Barry AO, Pretat L, Al Moussawi K, Desnues B, Capo C, Kornfeld H, Mege J-L. IL-16 promotes T. whipplei replication by inhibiting phagosome conversion and modulating macrophage activation. PLoS One 2010;5:e13561. https://doi.org/10.1371/journal.pone.0013561
[24] Gola A, Dorrington MG, Speranza E, Sala C, Shih RM, Radtke AJ, Wong HS, Baptista AP, Hernandez JM, Castellani G. Commensal-driven immune zonation of the liver promotes host defence. Nature 2021;589:131–6.
[25] Gola A, Dorrington MG, Speranza E, Sala C, Shih RM, Radtke AJ, Wong HS, Baptista AP, Hernandez JM, Castellani G, et al. Commensal-driven immune zonation of the liver promotes host defence. Nature 2021;589:131–6. https://doi.org/10.1038/s41586-020-2977-2
[26] Gualdi R, Bossard P, Zheng M, Hamada Y, Coleman JR, Zaret KS. Hepatic specification of the gut endoderm in vitro: cell signaling and transcriptional control. Genes Dev 1996;10:1670–82.

[27] Guilliams M, Bonnardel J, Haest B, Vanderborght B, Wagner C, Remmerie A, Bujko A, Martens L, Thoné T, Browaeys R, et al. Spatial proteogenomics reveals distinct and evolutionarily conserved hepatic macrophage niches. Cell 2022:*185*. https://doi.org/10.1016/j.cell.2021.12.018
[28] Haghikia A, Zimmermann F, Schumann P, Jasina A, Roessler J, Schmidt D, Heinze P, Kaisler J, Nageswaran V, Aigner A, et al. Propionate attenuates atherosclerosis by immune-dependent regulation of intestinal cholesterol metabolism. Eur Heart J 2022;43:518–33. https://doi.org/10.1093/eurheartj/ehab644
[29] Halpern KB, Shenhav R, Massalha H, Toth B, Egozi A, Massasa EE, Medgalia C, David E, Giladi A, Moor AE, et al. Paired-cell sequencing enables spatial gene expression mapping of liver endothelial cells. Nat Biotechnol 2018;36:962–70. https://doi.org/10.1038/nbt.4231
[30] Halpern KB, Shenhav R, Matcovitch-Natan O, Toth B, Lemze D, Golan M, Massasa EE, Baydatch S, Landen S, Moor AE, et al. Single-cell spatial reconstruction reveals global division of labour in the mammalian liver. Nature 2017;542:352–6. https://doi.org/10.1038/nature21065
[31] Han L, Wei X, Liu C, Volpe G, Zhuang Z, Zou X, Wang Z, Pan T, Yuan Y, Zhang X, et al. Cell transcriptomic atlas of the non-human primate Macaca fascicularis. Nature 2022;604:723–31. https://doi.org/10.1038/s41586-022-04587-3
[32] Hanke T, Mitnacht R, Boyd R, Hünig T. Induction of interleukin 2 receptor beta chain expression by self-recognition in the thymus. J Exp Med 1994;180:1629–36.
[33] Ishida T, Kundu RK, Yang E, Hirata K-i, Ho Y-D, Quertermous T. Targeted disruption of endothelial cell-selective adhesion molecule inhibits angiogenic processes in vitro and in vivo. J Biol Chem 2003;278:34598–604.
[34] Jin S, Guerrero-Juarez CF, Zhang L, Chang I, Ramos R, Kuan C-H, Myung P, Plikus MV, Nie Q. Inference and analysis of cell-cell communication using CellChat. Nat Commun 2021;12:1088. https://doi.org/10.1038/s41467-021-21246-9
[35] Juanola O, Hassan M, Kumar P, Yilmaz B, Keller I, Simillion C, Engelmann C, Tacke F, Dufour J-F, De Gottardi A, Moghadamrad S. Intestinal microbiota drives cholestasis-induced specific hepatic gene expression patterns. Gut Microbes 2021:*13*. https://doi.org/10.1080/19490976.2021.1911534
[36] Kang DJ, Hylemon PB, Gillevet PM, Sartor RB, Betrapally NS, Kakiyama G, Sikaroodi M, Takei H, Nittono H, Zhou H, et al. Gut microbial composition can differentially regulate bile acid synthesis in humanized mice. Hepatol Commun 2017;1:61–70. https://doi.org/10.1002/hep4.1020
[37] Kietzmann T. Liver zonation in health and disease: hypoxia and hypoxia-inducible transcription factors as concert masters. Int J Mol Sci 2019:*20*. https://doi.org/10.3390/ijms20092347
[38] Kim J-E, Fei L, Yin W-C, Coquenlorge S, Rao-Bhatia A, Zhang X, Shi SSW, Lee JH, Hahn NA, Rizvi W. Single cell and genetic analyses reveal conserved populations and signaling mechanisms of gastrointestinal stromal niches. Nat Commun 2020;11:334.
[39] Kosugi A, Saitoh S, Narumiya S, Miyake K, Hamaoka T. Activation-induced expression of thymic shared antigen-1 on T lymphocytes and its inhibitory role for TCR-mediated IL-2 production. Int Immunol 1994;6:1967–76.
[40] Kubinak JL, Stephens WZ, Soto R, Petersen C, Chiaro T, Gogokhia L, Bell R, Ajami NJ, Petrosino JF, Morrison L, et al. MHC variation sculpts individualized microbial communities that control susceptibility to enteric infection. Nat Commun 2015;6:8642. https://doi.org/10.1038/ncomms9642
[41] McDonald B, Zucoloto AZ, Yu I-L, Burkhard R, Brown K, Geuking MB, McCoy KD. Programing of an intravascular immune firewall by the gut microbiota protects against pathogen dissemination during infection. Cell Host Microbe 2020:*28*. https://doi.org/10.1016/j.chom.2020.07.014
[42] McDonald BD, Jabri B, Bendelac A. Diverse developmental pathways of intestinal intraepithelial lymphocytes. Nat Rev Immunol 2018;18:514–25. https://doi.org/10.1038/s41577-018-0013-7
[43] Moriel N, Senel E, Friedman N, Rajewsky N, Karaiskos N, Nitzan M. NovoSpaRc: flexible spatial reconstruction of single-cell gene expression with optimal transport. Nat Protoc 2021;16:4177–200. https://doi.org/10.1038/s41596-021-00573-7
[44] Moro-Sibilot L, Blanc P, Taillardet M, Bardel E, Couillault C, Boschetti G, Traverse-Glehen A, Defrance T, Kaiserlian D, Dubois B. Mouse and Human Liver Contain immunoglobulin a-secreting cells originating from peyer's patches and directed against intestinal antigens. Gastroenterology 2016;151:311–23. https://doi.org/10.1053/j.gastro.2016.04.014
[45] Nault R, Fader KA, Bhattacharya S, Zacharewski TR. Single-nuclei RNA sequencing assessment of the hepatic effects of 2,3,7,8-Tetrachlorodibenzo-p-dioxin. Cell Mol Gastroenterol Hepatol 2021;11:147–59. https://doi.org/10.1016/j.jcmgh.2020.07.012
[46] Noda S, Kosugi A, Saitoh S, Narumiya S, Hamaoka T. Protection from anti-TCR/CD3-induced apoptosis in immature thymocytes by a signal through thymic shared antigen-1/stem cell antigen-2. J Exp Med 1996;183:2355–60.
[47] Orsenigo F, Giampietro C, Ferrari A, Corada M, Galaup A, Sigismund S, Ristagno G, Maddaluno L, Koh GY, Franco D, et al. Phosphorylation of VE-cadherin is modulated by haemodynamic forces and contributes to the regulation of vascular permeability in vivo. Nat Commun 2012;3:1208. https://doi.org/10.1038/ncomms2199
[48] Ortiz C, Navarro JF, Jurek A, Märtin A, Lundeberg J, Meletis K. Molecular atlas of the adult mouse brain. Sci Adv 2020;6:eabb3446. https://doi.org/10.1126/sciadv.abb3446
[49] Ramachandran P, Matchett KP, Dobie R, Wilson-Kanamori JR, Henderson NC. Single-cell technologies in hepatology: new insights into liver biology and disease pathogenesis. Nat Rev Gastroenterol Hepatol 2020;17:457–72. https://doi.org/10.1038/s41575-020-0304-x
[50] Roland MM, Mohammed AD, Kubinak JL. How MHCII signaling promotes benign host-microbiota interactions. PLoS Pathog 2020;16:e1008558. https://doi.org/10.1371/journal.ppat.1008558
[51] Saitoh S, Kosugi A, Noda S, Yamamoto N, Ogata M, Minami Y, Miyake K, Hamaoka T. Modulation of TCR-mediated signaling pathway by thymic shared antigen-1 (TSA-1)/stem cell antigen-2 (Sca-2). J Immunol 1995;155:5574–81.
[52] Sakai M, Troutman TD, Seidman JS, Ouyang Z, Spann NJ, Abe Y, Ego KM, Bruni CM, Deng Z, Schlachetzki JCM, et al. Liver-derived signals sequentially reprogram myeloid enhancers to initiate and maintain kupffer cell identity. Immunity 2019:*51*. https://doi.org/10.1016/j.immuni.2019.09.002
[53] Sarrias M-R, Farnós M, Mota R, Sánchez-Barbero F, Ibáñez A, Gimferrer I, Vera J, Fenutría R, Casals C, Yélamos J, Lozano F. CD6 binds to pathogen-associated molecular patterns and protects from LPS-induced septic shock. Proc Natl Acad Sci USA 2007;104:11724–9.
[54] Sun R, Xu C, Feng B, Gao X, Liu Z. Critical roles of bile acids in regulating intestinal mucosal immune responses. 17562848211018098 Ther Adv Gastroenterol 2021;14. https://doi.org/10.1177/17562848211018098
[55] Tarasov A, Vilella AJ, Cuppen E, Nijman IJ, Prins P. Sambamba: fast processing of NGS alignment formats. Bioinforma (Oxf, Engl) 2015;31:2032–4. https://doi.org/10.1093/bioinformatics/btv098
[56] Tirosh A, Calay ES, Tuncman G, Claiborn KC, Inouye KE, Eguchi K, Alcala M, Rathaus M, Hollander KS, Ron I, et al. The short-chain fatty acid propionate increases glucagon and FABP4 production, impairing insulin action in mice and humans. Sci Transl Med 2019:*11*. https://doi.org/10.1126/scitranslmed.aav0120
[57] Tripathi A, Debelius J, Brenner DA, Karin M, Loomba R, Schnabl B, Knight R. The gut-liver axis and the intersection with the microbiome. Nat Rev Gastroenterol Hepatol 2018;15:397–411. https://doi.org/10.1038/s41575-018-0011-z
[58] van Oosten M, van de Bilt E, de Vries HE, van Berkel TJ, Kuiper J. Vascular adhesion molecule-1 and intercellular adhesion molecule-1 expression on rat liver cells after lipopolysaccharide administration in vivo. Hepatology 1995;22:1538–46.
[59] Wahlström A, Sayin SI, Marschall H-U, Bäckhed F. Intestinal crosstalk between bile acids and microbiota and its impact on host metabolism. Cell Metab 2016;24:41–50. https://doi.org/10.1016/j.cmet.2016.05.005
[60] Wang M, Hu Q, Lv T, Wang Y, Lan Q, Xiang R, Tu Z, Wei Y, Han K, Shi C, et al. High-resolution 3D spatiotemporal transcriptomic maps of developing Drosophila embryos and larvae. Dev Cell 2022:*57*. https://doi.org/10.1016/j.devcel.2022.04.006
[61] Wu Z, Cheng W, Wang Z, Feng S, Zou H, Tan X, Yang Y, Wang Y, Zhang H, Dong M, et al. Intestinal microbiota and serum metabolic profile responded to two nutritional different diets in mice. Front Nutr 2021;8:813757. https://doi.org/10.3389/fnut.2021.813757
[62] Xia K, Sun H-X, Li J, Li J, Zhao Y, Chen L, Qin C, Chen R, Chen Z, Liu G, et al. The single-cell stereo-seq reveals region-specific cell subtypes and transcriptome profiling in Arabidopsis leaves. Dev Cell 2022;57. https://doi.org/10.1016/j.devcel.2022.04.011
[63] Xiong X, Kuang H, Ansari S, Liu T, Gong J, Wang S, Zhao X-Y, Ji Y, Li C, Guo L, et al. Landscape of intercellular crosstalk in healthy and NASH liver revealed by single-cell secretome gene analysis. e645 Mol Cell 2019;75:644–60. https://doi.org/10.1016/j.molcel.2019.07.028
[64] Yang M, Ma F, Guan M. Role of steroid hormones in the pathogenesis of non-alcoholic fatty liver disease. Metabolites 2021:*11*. https://doi.org/10.3390/metabo11050320
[65] Young MD, Behjati S. SoupX removes ambient RNA contamination from droplet-based single-cell RNA sequencing data. Gigascience 2020:*9*. https://doi.org/10.1093/gigascience/giaa151